Directed Bridging Methods for Fast Atomistic Monte Carlo Simulations of Bulk Polymers

Alfred Uhlherr,*,† Vlasis G. Mavrantzas,‡ Manolis Doxastakis,‡ and Doros N. Theodorou‡

CSIRO Molecular Science, Bag 10, Clayton South, Victoria 3169, Australia; Department of Chemical Engineering, University of Patras, GR 26500 Patras, Greece; and Institute of Chemical Engineering and High-Temperature Chemical Processes, GR 26500 Patras, Greece

Received February 5, 2001; Revised Manuscript Received August 14, 2001

ABSTRACT: A new class of Monte Carlo algorithms for atomistic simulation of genuine high polymer systems is proposed. Derivations of two of these algorithms, dubbed "directed internal bridging" (DIB) and "directed end bridging" (DEB), are presented. Their performance is analyzed in detail, using linear united-atom polyethylene of mean chain length C_{1000} as an archetypal entangled polymer melt. It is shown in particular that the DEB algorithm is substantially faster than previous alternatives in equilibrating such melts on all length scales. Used in a suitable protocol of mixed Monte Carlo moves, it thus provides the most powerful means available to date for quantitative molecular simulation of such materials, and makes atomic level characterization of realistic high polymer melts a feasible proposition.

Introduction

Molecular simulation methods[1−4] have already proved to be of immense value in pure and applied condensed matter research.[5,6] As computing performance continues to grow with each passing year, so the popularity and usefulness of molecular simulations will also continue to increase. In particular, it is likely that they will be central to the development of new polymeric materials, where there is still substantial scope for improvement of our understanding of the subtle connections between detailed chemical structure and macroscopic properties.[7]

In principle, it should be possible to perform molecular simulation of polymers with (i) full atomic detail, (ii) realistic (high) molecular weights, and (iii) full self-consistency in the chain configurations (i.e., structure governed by actual chemical environment rather than by ad hoc initial guess). In practice, the prohibitively long relaxation times associated with large scale chain configurations severely limits our abilities to attain these three goals simultaneously. Using current techniques and computer hardware, only two of the three goals can be attained in any given simulation. The net result has been a concentration of work on subpolymeric oligomers, nonequilibrium homopolymer glasses, and generic physics of simple "coarse-grained" model polymers,[6−10] rather than more realistic, truly polymeric materials.

Hence, considerable effort has been devoted to developing new Monte Carlo (MC) algorithms capable of more efficient sampling of bulk long chain configurations.[11] The emphasis to date has been on equilibrium simulation of high polymer melts. This capability is obviously of great importance in its own right. It also provides the necessary starting point for characterizing melts under nonequilibrium conditions, such as the flow regimes utilized in polymer processing,[12] as well as glassy and semicrystalline solid polymers[13,14] which are commonly produced via the melt state.

Many of the familiar MC algorithms used in these atomistic polymer simulations, such as the reptation, end rotation, flip, and volume fluctuation moves, have been described in detail elsewhere.[11,15] The concerted rotation (ConRot) algorithm[16] and its variants[15,17−19] address the sampling of the torsional degrees of freedom in short internal sections of chain molecules with fixed or stiff bond length and angle constraints. The configuration bias (CB) algorithm[20,21] performs torsional sampling of arbitrarily long end sections of chains, and works best for moderate chain lengths and densities. Recently the internal configuration bias[22] (ICB) and self-adapting fixed end point configuration bias[23] (SAFE−CB) methods have been devised, combining the ConRot and CB philosophies to enable sampling of arbitrarily long internal chain sections.

A powerful extension of the ConRot concept is the end-bridging (EB) algorithm.[24,15] This uses a similar geometrical operation to create an intermolecular trimer bridge, thus altering the bond connectivity of the polymer system. In marked contrast to other molecular simulation methods, EB equilibration rate is an increasing function of chain length. Hence EB simulations are orders of magnitude faster for truly polymeric (i.e., entangled) materials.

The main limits on the effectiveness of EB are as follows:

- a very low acceptance ratio (around 0.1%), due to the torsional strain associated with connecting monomers on different chains via a trimer bridge;
- the propensity for instant move reversal or "shuttling", caused by the relatively small number of feasible candidate EB moves available at any one time.

These limitations become increasingly acute for more complex chemical structures,[25] such as monomers with bulky side groups or large persistence lengths.

Both of these limitations can in principle be addressed by a hypothetical "extended EB" involving a longer section of chain. Given that ICB and SAFE−CB are

* To whom correspondence should be addressed. Telephone: + 61 3 9545 8107. Fax: + 61 3 9545 2446. E-mail: a.uhlherr@molsci.csiro.au.

† CSIRO Molecular Science.

‡ University of Patras and Institute of Chemical Engineering and High-Temperature Chemical Processes.

10.1021/ma0102060 CCC: $20.00
Published on Web 10/18/2001

analogous extensions of ConRot, a similar extension to EB is obviously an attractive proposition.[22,23] Such an extension is the main subject of the present work.

It is worth highlighting some of the advantages and disadvantages of variable connectivity MC simulations compared with standard methods such as molecular dynamics (MD). The obvious advantage is the ability to calculate static structural and thermodynamic data for polymer systems that are utterly inaccessible to MD techniques. The simulated systems are polydisperse, with a controlled molecular weight distribution, which can be made to match that of an experimentally prepared material. In principle, there is no maximum limit to the polydispersity. In practice, high polydispersities comparable to commercial grade polyolefins are difficult, simply because implementing a high molecular weight "tail" requires a very large number of atoms in the simulated system. Low polydispersities do not present difficulty; MC simulation can address polydispersities below those accessible experimentally by the most advanced anionic polymerization techniques. The other advantage of polydisperse simulations is that chain length dependencies can be calculated from a single simulation run. Note that enforced polydispersity is unsuitable for some applications, such as biopolymers with specific monomer sequences.

The obvious disadvantage of MC simulation with dynamically unphysical moves is the inability to calculate dynamic data such as diffusion coefficients. In practice, this disadvantage is not as great as is commonly perceived. The MC techniques can readily be combined with MD to obtain short time dynamic data for well equilibrated configurations,[26] and substantial advances in combining MC with irreversible thermodynamics formalisms for calculation of viscoelastic properties are in progress.[12,27,28] It appears unlikely that pure MD simulations will ever produce quantitative dynamic data on realistic high polymer melts that cannot be obtained equally well, or better, by MC or combined MC/MD simulation.

Perhaps the most serious drawback of atomistic polymer MC simulations, notably those involving variable connectivity, is their sheer complexity. Codes implementing these algorithms are much larger than MD codes, or simple MC codes for coarse-grained chains. Many generalized MD codes, suitable for routine atomistic simulation of short-chain polymers, are now available either commercially or in the public domain. Conversely, development and testing of new MC algorithms requires substantial effort, often for little reward,[29,30] resulting in incremental progress over the past decade. It is also the main reason for focusing on very simple polymers, notably the united-atom "polybead" model for polyethylene. Such a model, while quantitative, is strictly speaking not atomistic. However, it does contain the key elements defining the nature of the computational problem for all-atom polymer simulations, namely dense packing and stiff bond length and angle constraints. Extension to all-atom simulations (e.g., polyethylene with explicit hydrogens)[31] or more complex chemical constitutions (e.g., polyisoprene)[25] involves further programming complexity, and 1−2 orders of magnitude loss of performance. This loss is dwarfed by the dramatically improved scaling for long chains obtained by algorithms such as those considered here. Hence, as soon as a near-optimal algorithm is identified, development of a generalized all-atom implementation would become not only feasible but also highly desirable.

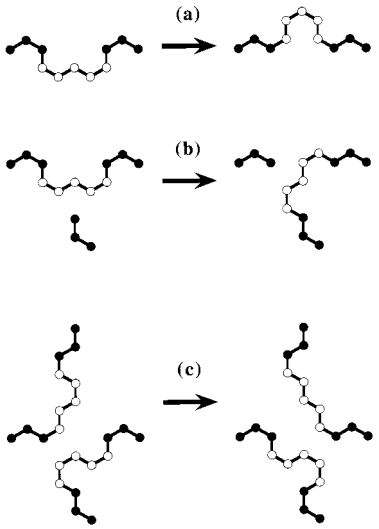

Figure 1. Schematic representation of different types of bridging moves for atomistic Monte Carlo simulation of chain molecular systems: (a) internal bridging; (b) end bridging; (c) cross-bridging. Shaded atoms are held fixed during the course of each move. These examples use simple linear chains and bridging segments of length $l = 5$.

Algorithms

Figure 1 shows a pictorial representation of several different kinds of rebridging moves that can be implemented in Monte Carlo simulations of chain molecule systems. We propose a family of MC moves which can reform such bridges of arbitrary length, l, while fixing the associated bond lengths (and angles) to constant or preassigned values. This can be accomplished by sequentially rebuilding the bridge, one atom at a time, using a configuration bias random walk, until the imposed geometric constraints limit the number of possible configurations for the remaining atoms to a finite value. All of these remaining configurations are then identified by solving the associated geometric constraint equations, and one of these configurations is chosen by a suitable weighting procedure. For linear chain sections, these geometric constraint equations correspond to the construction of a bridging trimer. Since a Monte Carlo scheme has to satisfy the detailed balance or "microscopic reversibility" requirement[2] in order to correctly sample the configuration space, the original configuration of the bridge also needs to be regenerated, step by step, to calculate the necessary weighting terms used to determine whether the new configuration is accepted.

When successive atoms in the bridge are regrown, it is of course necessary to ensure that they are regrown in such a fashion that the last bridging atom reconnects with the fixed atom that forms the end point of the bridge. Hence an additional term is introduced into the configuration bias procedure, to encourage the growth of each atom in the correct direction. We use the term "directed bridging" to describe this general principle, which has also been invoked for lattice and freely jointed chains.[32,33]

From Figure 1 we may identify three examples of the directed bridging approach. The simplest example is a "directed internal bridging" (DIB) algorithm, where an internal section of a single chain is rebridged. The

second example is a "directed end-bridging" (DEB) algorithm, whereby the end of one chain "attacks" an interior segment of another chain, thus altering the connectivity of the atoms in both chains. Such an algorithm creates a polydisperse sample, and is expected to give very efficient configurational sampling. A third example is a "directed cross-bridging" (DXB) algorithm, where two new bridges are formed across a pair of chains. Cross-bridging moves are an extremely attractive proposition, since they can in principle be applied to arbitrarily high molecular weight chains (e.g., networks) and monodisperse or polydisperse samples. In the polydisperse case, the number of candidate cross-bridging moves greatly exceeds the number of candidate end-bridging moves. Cross-bridging moves have been used successfully in simulations of simpler systems, for example in (semicrystalline) polyethylene in the absence of torsional barriers,[14] and in (monodisperse) simulations of FENE chains.[34] However, rebridging more than one chain in a single MC move leads to very low acceptances when realistic interatomic potentials are used.[30] Hence, while implementation of DXB is in progress, in this work we will focus on DIB and DEB.

The basis of most Monte Carlo condensed matter simulations is the familiar Metropolis method.[35] This generates a Markov chain of configurational states of the molecular system, whereby each successive state is generated by randomly accepting or rejecting a trial move with a probability that depends on the statistical weight of the state (i.e., importance sampling). For a molecular system at thermodynamic equilibrium at temperature T, the acceptance probability[35,2] for the isochoric transition from an old state ξ to a new state ξ^* can be written in the form

$$\mathrm{Acc}_{\xi \to \xi^*} = \min\left(1, \frac{S_{\xi^* \to \xi}}{S_{\xi \to \xi^*}} \exp[-\beta(U(\xi^*) - U(\xi))]\right) \quad (1)$$

where $U(\xi)$ is the total potential energy of state ξ, $\beta = (1/k_B T)$ is the reduced temperature and k_B is Boltzmann's constant. $S_{\xi \to \xi^*}$ is used here to denote the propositional probability for choosing the new state ξ^* as the selected target for the trial move, while $S_{\xi^* \to \xi}$ is the corresponding probability for the reverse transition. The key to a new MC algorithm is to derive an analytical expression for the ratio of these probabilities. Note that in the original Metropolis derivation, where individual particles are moved by small isotropic random displacements, this ratio is equal to unity.

For simplicity, we will describe the derivation of the DIB algorithm for linear chains, in the absence of side groups, branches, or cross-links. It is convenient to identify the configurational state of the whole system ξ with the configurational state of the l atoms in the bridge, since any energy change in the whole system is associated with these displaced atoms. We may then write the total energy of this configuration as a sum of internal and external contributions due to each atom,

$$U(\xi) = \sum_{i=1}^{l} u^{\mathrm{int}}(\mathbf{x}_i) + \sum_{i=1}^{l} u^{\mathrm{ext}}(\mathbf{x}_i) \quad (2)$$

where $\mathbf{x}_i$ is the Cartesian coordinate vector of atom i. For simulating chain molecule systems, u^{ext} typically corresponds to nonbond energy terms, such as dispersion and electrostatic interactions, while u^{int} corresponds to bonding interactions, such as stretching, bending, and torsion energies.

The DIB move consists of a combination of a configuration bias step and a trimer rebridging step. Hence we may further split the set of l bridging atoms ξ into a set of $l - 3$ walker atoms, χ, and a set of three trimer atoms, ψ. This allows us to rewrite the propositional probability ratio in the form

$$\frac{S_{\xi^* \to \xi}}{S_{\xi \to \xi^*}} = \frac{S_{\chi^* \to \chi} S_{\psi^* \to \psi}}{S_{\chi \to \chi^*} S_{\psi \to \psi^*}} \quad (3)$$

corresponding to separate construction of χ and ψ.

The new configuration of χ^* is constructed by configuration bias, for which the propositional probability may be written in the form

$$\frac{S_{\chi^* \to \chi}}{S_{\chi \to \chi^*}} = \frac{W(\chi^*) \exp(\beta V(\chi^*))}{W(\chi) \exp(\beta V(\chi))} \quad (4)$$

Here V is the bias energy used in the regrowth, which may also be written in terms of internal and external contributions for each atom,

$$V(\chi) = \sum_{i=1}^{l-3} v^{\mathrm{int}}(\mathbf{x}_i) + \sum_{i=1}^{l-3} v^{\mathrm{ext}}(\mathbf{x}_i) \quad (5)$$

W denotes the continuum Rosenbluth weight,[2,36] given by

$$W(\chi) = \prod_{i=1}^{l-3} \frac{1}{n_q} \sum_{q=1}^{n_q} \exp(-\beta v^{\mathrm{ext}}(\mathbf{x}_{i,q})) \quad (6)$$

where $\mathbf{x}_{i,q}$ is the qth of n_q trial configurations of atom i, which are generated randomly with Boltzmann weighting $\exp(-\beta v^{\mathrm{int}}(\mathbf{x}_{i,q}))$, and from which the new coordinates of i are selected randomly with weighting $\exp(-\beta v^{\mathrm{ext}}(\mathbf{x}_{i,q}))$.

Once the new positions of the $l - 3$ walker atoms χ are determined, the bridge may be closed by generating new positions for the 3 trimer atoms ψ. For a simple search for a single trimer solution, the necessary expression[24,22] for the propositional probabilities is

$$\frac{S_{\psi^* \to \psi}}{S_{\psi \to \psi^*}} = \frac{J(\psi^*)}{J(\psi)} \quad (7)$$

where J denotes the Jacobian determinant for the transformation between Cartesian and constraint coordinate systems. Here we instead identify all possible trimer solutions by an exhaustive search,[16,15] as used in the ConRot method. The corresponding ratio of probabilities[16] is given by

$$\frac{S_{\psi^* \to \psi}}{S_{\psi \to \psi^*}} = \frac{J(\psi^*)\alpha(\psi)}{J(\psi)\alpha(\psi^*)} \quad (8)$$

where α is the probability of selecting a particular trimer solution, which is typically done using Boltzmann weighting, i.e.

$$\alpha(\psi) = \frac{\exp(-\beta U(\psi))}{\sum_{q=1}^{n_q} \exp(-\beta U(\psi_q))} \tag{9}$$

If we use the temporary indices *a*, *b*, *c*, *d*, *e*, *f*, and *g* to denote the sequence of seven atoms centered on the trimer, then the Jacobian is given by[15]

$$J(\psi) = \det\left(\frac{\partial(l_{bc},l_{cd},l_{de},l_{ef},l_{ac},l_{bd},l_{ce},l_{df},l_{eg})}{\partial(\mathbf{x}_c,\mathbf{x}_d,\mathbf{x}_e)}\right)^{-1} \tag{10}$$

where l_{ij} denotes the predefined distance between atoms *i* and *j*. The partial derivatives for coordinate $\mathbf{x}_k = (x_k, y_k, z_k)$ can be written in the form

$$\frac{\partial l_{ij}}{\partial x_k} = \begin{cases} \dfrac{x_i - x_j}{l_{ij}}, & k = i \\ \dfrac{-(x_i - x_j)}{l_{ij}}, & k = j \\ 0, & k \neq i,j \end{cases} \tag{11}$$

with equivalent expressions for the y_k and z_k directions.

We can now write the final expression for the acceptance probability for DIB moves as

$$\mathrm{Acc}_{\xi\to\xi^*} = \min\left(1, \frac{W(\chi^*)\exp(\beta V(\chi^*))\exp(-\beta U(\xi^*))J(\psi^*)\alpha(\psi)}{W(\chi)\exp(\beta V(\chi))\exp(-\beta U(\xi))J(\psi)\alpha(\psi^*)}\right) \tag{12}$$

This formalism is similar to that for the original ICB algorithm,[22] with the main differences being associated with the trimer step. An analogous formalism is also used in the SAFE−CB algorithm.[23] Note that variable bond angles are optional for ICB and DIB, whereas for SAFE−CB they are required; the distinction is minor given that most quantitative potentials for polymers incorporate variable bond angles.

Just as DIB can be considered an extension of the ConRot algorithm, DEB can be considered an extension of the original end-bridging (EB) algorithm. The propositional probability ratio for end-bridging moves[24] can be written as

$$\frac{S_{\psi^*\to\psi}}{S_{\psi\to\psi^*}} = \frac{\gamma_{\psi\to\psi^*}J(\psi^*)\alpha(\psi)}{\gamma_{\psi^*\to\psi}J(\psi)\alpha(\psi^*)} \tag{13}$$

where $\gamma_{\psi\to\psi^*}$ and $\gamma_{\psi^*\to\psi}$ represent the number of candidate target atoms for the chain end in the forward and reverse moves. This attacking chain end is selected at random. As the DEB move is otherwise equivalent to the DIB move, the DEB acceptance ratio may then be written as

$$\mathrm{Acc}_{\xi\to\xi^*} = \min\left(1, \frac{W(\chi^*)\exp(\beta V(\chi^*))\exp(-\beta U(\xi^*))\gamma_{\psi\to\psi^*}J(\psi^*)\alpha(\psi)}{W(\chi)\exp(\beta V(\chi))\exp(-\beta U(\xi))\gamma_{\psi^*\to\psi}J(\psi)\alpha(\psi^*)}\right) \tag{14}$$

Note that this expression corresponds to equal probabilities (and chemical potentials μ^*) for all chain lengths. Simply discarding moves that generate chains outside the specified minimum and maximum chain length bounds then leads to a uniform rectangular molecular weight distribution.

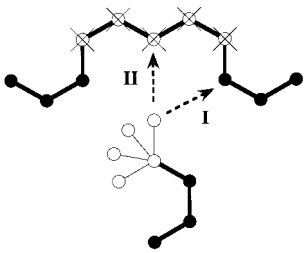

Figure 2. Schematic representation of a directed end-bridging Monte Carlo move, for the case $l = 5$. Shaded atoms are held fixed during the course of the move. Crossed atoms are deleted and replaced by atoms grown from the end of the other chain using configuration bias. For directing potential I, selection from the trial positions for each newly grown atom is biased toward the first fixed atom in the target chain. For directing potential II, the bias is directed toward the *old* position of the first of the three atoms in the closing trimer.

So far we have not yet described the form of the bias potential *V*. Usually in CB, the bias potential is simply equal to *U*, the actual potential.[2] Here we use it as a convenient means to introduce a fictitious energy term to direct the regrowth of these bridging atoms. Note that by using the same fictitious potential in constructing the forward and reverse moves according to eqs 12 and 14, we ensure that the correct equilibrium sampling of configurational states according to the real potential *U* is maintained. The internal component of the fictitious potential is chosen to be the same as the real potential, i.e.

$$v^{\mathrm{int}}(\mathbf{x}_i) = u^{\mathrm{int}}(\mathbf{x}_i) \tag{15}$$

For the external component of the fictitious potential, a finite extensible nonlinear elastic (FENE) "spring" term is added,[22] to give the form

$$v^{\mathrm{ext}}(\mathbf{x}_i) = u^{\mathrm{ext}}(\mathbf{x}_i) - \frac{1}{2}CR_{ij}^2 \ln\left(1 - \left(\frac{r_{ij}}{R_{ij}}\right)^2\right) \tag{16}$$

where r_{ij} is the distance from the regrown atom *i* to a suitable attractor site *j*. Previously optimized values[22] of the constant terms are used, namely $C/k_B = 10$ K and $R_{ij} = 1.275(j + 1 - i)$ Å.

When specifying the attractor for the directed regrowth, two alternative formulations are considered here. These are illustrated in Figure 2 for the case of a DEB move. In variant I, regrown atoms are directed toward the bridge end point, i.e., the first fixed atom at the opposite end of the bridge. In variant II, regrown atoms are directed toward the *old* coordinates of the first trimer atom. The intention in variant II is to boost acceptance by encouraging the formation of a new trimer that is as similar as possible to the old trimer. When evaluating the Rosenbluth weights for the reverse move, detailed balance is enforced by directing the regrowth of atoms in the original configuration toward the *new* coordinates of the first trimer atom. Finally, simulations with no fictitious directing component to the bias potential (i.e., $C = 0$) were also performed for comparison purposes. Without this directing potential, the bias potential *V* becomes equal to the actual potential *U* for both χ and ψ segments. The acceptance criterion for DIB moves then simplifies to

$$\mathrm{Acc}_{\xi\to\xi^*} = \min\left(1, \frac{W(\chi^*)\exp(-\beta U(\psi^*))J(\psi^*)\alpha(\psi)}{W(\chi)\exp(-\beta U(\psi))J(\psi)\alpha(\psi^*)}\right) \quad (17)$$

while that for DEB moves can likewise be reduced to

$$\mathrm{Acc}_{\xi\to\xi^*} = \min\left(1, \frac{W(\chi^*)\exp(-\beta U(\psi^*))\gamma_{\psi\to\psi^*}J(\psi^*)\alpha(\psi)}{W(\chi)\exp(-\beta U(\psi))\gamma_{\psi^*\to\psi}J(\psi)\alpha(\psi^*)}\right) \quad (18)$$

Run Details

To assess performance aspects of the different MC moves, we consider a linear polyethylene melt at a temperature $T = 450$ K and a pressure $p = 1$atm. The system consists of $N = 24\,000$ united atoms contained in $n = 24$ chains, giving a number-average chain length of 1000 mer units or approximately 14000 g mol^{-1}. The chain length is constrained to a rectangular distribution ranging from 600 to 1400, corresponding to a reduced width $\Delta = 0.4$, or a polydispersity index $Z = 1.053$. The combination of relatively high molecular weight and large system size helps to minimize any overlap or confusion between local and global relaxation properties.

The polyethylene model is the same as that used previously.[15] CH_2 and CH_3 units are separated by fixed bond lengths of 1.54 Å and treated as equivalent, spherically symmetric united atoms, interacting via a Lennard-Jones nonbond potential of the form

$$u_{\mathrm{LJ}}(r_{ij}) = 4\epsilon\left(\left(\frac{\sigma}{r_{ij}}\right)^{12} - \left(\frac{\sigma}{r_{ij}}\right)^{6}\right) \quad (19)$$

where r_{ij} is the distance between atoms i and j. The well depth ϵ/k_B and the interaction diameter σ are set to 49.3 K and 3.94 Å, respectively. Explicit pairwise interactions are truncated at 2.3σ and augmented by standard long range corrections.[1]

Three-body interactions are specified by a harmonic bond-bending potential,[37]

$$u_{\mathrm{bend}}(\theta_i) = \frac{1}{2}k_\theta(\theta_i - \theta_0)^2 \quad (20)$$

with a bending stiffness $k_\theta/k_B = 57\,950$ K·rad^{-2} and equilibrium angle $\theta_0 = 112°$. The torsion term is of the Ryckaert−Bellemans functional form,[38]

$$u_{\mathrm{tor}}(\phi_i) = \sum_{m=0}^{5} A_m \cos^m(\phi_i) \quad (21)$$

with coefficients $A_m/k_B = +1116, +1462, -1578, -368, +3156$, and -3788 K respectively for $m = 0-5$. For the DIB and DEB moves, the $l - 3$ walker atoms are regrown by Rosenbluth sampling (eq 6) using $n_q = 20$ trial positions for each atom, with new bond angles and torsion angles generated by Boltzmann-weighted sampling of the associated potential functions (eqs 20 and 21).

The potential functions above can be matched to those in the algorithm derivation by defining θ_i as the bond angle centered on atom i, and ϕ_i as the torsion angle about the bond between atoms i and $i + 1$. Then, for $i < l - 1$, the internal energy can be defined simply as

$$u^{\mathrm{int}}(\mathbf{x}_i) = u_{\mathrm{bend}}(\theta_{i-1}) + u_{\mathrm{tor}}(\phi_{i-2}) \quad (22)$$

For $i = l$, additional bond and torsion angles associated with the bridge closure need to be included, hence

$$u^{\mathrm{int}}(\mathbf{x}_l) = \sum_{k=l-1}^{l+1} u_{\mathrm{bend}}(\theta_k) + \sum_{k=l-2}^{l+1} u_{\mathrm{tor}}(\phi_k) \quad (23)$$

Similarly the external energy for each atom can be expressed in terms of the pairwise Lennard-Jones contributions

$$u^{\mathrm{ext}}(\mathbf{x}_i) = \sum_j u_{\mathrm{LJ}}(r_{ij}) \quad (24)$$

where the sum over j is performed over all atoms outside the bridge, plus all atoms previously added to the bridge, $j < i$.

Table 1 lists the details of the polyethylene runs. The variable connectivity simulations were performed in the modified semigrand or $nN\mu^*pT$ ensemble.[24] In the absence of connectivity-altering EB or DEB moves, this reduces to the conventional isothermal−isobaric or NpT ensemble. In this context, reptations are not considered to be connectivity-altering moves. For DEB moves, the number of bridging atoms l is listed for each run. Where a range of l values is given, l for each move is sampled uniformly from this range. For DIB moves, the range of bridge lengths l is 3−8 in each run.

The data reported for all runs corresponds to 10 million iterations of attempted MC moves, analyzed over 100 intervals of 100 000 steps, starting from a configuration previously equilibrated by an extended EB simulation. All execution times are for a single NEC SX-4 processor under identical conditions, to aid the comparison process. The code makes extensive use of time-saving features such as a hierarchy of neighbor lists and prescreening of trial solutions, which have been detailed previously.[15]

A number of quantities are used here to characterize the performance of each MC simulation in terms of the rate of sampling of configuration space. These quantities are all time correlation functions, where the "time" variable t in this case is the number of MC steps.

The simplest is the atomic mean squared displacement function or MSD, given by

$$f_a(t) = \langle(\mathbf{x}_i(t + t_0) - \mathbf{x}_i(t_0))^2\rangle_{i,t_0} \quad (25)$$

where angular brackets are used to denote an ensemble average over all atoms i and multiple time origins t_o. The slope of this function can be used to infer an effective "diffusion" coefficient via the familiar Einstein equation.[1] Note that for reptation moves, the atoms are *not* renumbered, and hence only a single terminal atom is displaced. Thus, the MSD is still indicative of the rate of mass transport in the system, regardless of whether the transport process is dynamically realistic.

Other familiar measures of local relaxation include the bond vector and torsion angle autocorrelation functions.[11] In variable connectivity simulations such functions must be used with caution. First, one must account for specific bonds and angles becoming undefined and redefined as chain ends are continually being created and destroyed. Second, connectivity altering moves lead to renumbering of the atom identifiers, such that the order of atoms in a given chain section is frequently reversed. A series of stored atom coordinates is then no longer sufficient for quantifying the evolution of specific bond vectors and torsion angles.

Table 1. Run Details for the Monte Carlo Simulations

	reptation		rotation		flip		conrot		volfluc		EB		DIB		DEB			
run	mix %	acc %	mix %	acc %	mix %	acc %	mix %	acc %	mix %	acc %	mix %	acc %	mix %	acc %	mix %	acc %	*l*	CPU/s
A	6.0	6.5	6.0	16.0	6.0	76.7	32.0	7.3	0.10	3.0	49.9	0.091	0.0		0.0			24 913
B	6.0	7.4	6.0	16.7	6.0	76.6	31.9	7.9	0.10	3.3	0.0		0.0		50.0	0.082	$3-6^{(0)}$	29 725
C	6.0	7.8	6.0	16.8	6.0	76.6	31.9	8.0	0.10	3.2	0.0		0.0		50.0	0.118	3−6	34 661
D	6.0	6.9	6.0	16.2	6.0	76.8	31.9	7.9	0.10	3.0	0.0		0.0		50.0	0.052	$3-6^{(II)}$	31 735
E	12.0	7.3	12.0	16.4	12.0	76.7	63.8	7.9	0.20	3.3	0.0		0.0		0.0			43 622
F	12.0	7.2	12.0	16.4	12.0	76.6	0.0		0.20	3.4	0.0		63.8	6.7	0.0			69 551
G	6.0	6.2	6.0	15.7	6.0	76.6	0.0		0.10	3.0	50.0	0.097	31.9	6.7	0.0			45 391
H	6.0	8.0	6.0	17.0	6.0	76.5	31.9	8.0	0.10	3.3	0.0		0.0		50.0	0.113	5−7	42 031
I	6.0	7.8	6.0	16.9	6.0	76.6	0.0		0.10	3.1	0.0		31.9	6.7	50.0	0.118	5−7	51 232
J	6.0	7.3	6.0	16.3	6.0	76.7	31.9	7.9	0.10	3.5	0.0		0.0		50.0	0.053	3	24 014
K	6.0	7.6	6.0	16.6	6.0	76.6	31.9	8.1	0.10	3.2	0.0		0.0		50.0	0.124	4	30 903
L	6.0	7.6	6.0	16.7	6.0	76.7	31.9	8.0	0.10	3.1	0.0		0.0		50.0	0.150	5	35 571
M	6.0	8.0	6.0	17.0	6.0	76.6	31.9	8.1	0.10	3.1	0.0		0.0		50.0	0.122	6	39 479
N	6.0	8.2	6.0	16.9	6.0	76.5	31.9	8.0	0.10	2.7	0.0		0.0		50.0	0.052	7	39 659
O	10.8	6.6	10.8	15.9	10.8	76.7	57.4	7.8	0.18	3.1	0.0		0.0		10.0	0.117	3−6	41 730
P	9.6	7.4	9.6	16.5	9.6	76.6	51.0	7.9	0.16	2.5	0.0		0.0		20.0	0.113	3−6	39 616
Q	8.4	7.4	8.4	16.5	8.4	76.7	44.7	8.0	0.14	2.7	0.0		0.0		30.0	0.121	3−6	36 582
R	7.2	7.9	7.2	16.9	7.2	76.6	38.3	8.1	0.12	2.8	0.0		0.0		40.0	0.116	3−6	34 298
S	4.8	7.8	4.8	16.8	4.8	76.6	25.5	8.0	0.08	3.5	0.0		0.0		60.0	0.110	3−6	30 019
T	3.6	8.1	3.6	17.2	3.6	76.6	19.1	7.9	0.06	3.3	0.0		0.0		70.0	0.107	3−6	28 308
U	2.4	7.7	2.4	16.7	2.4	76.6	12.8	8.0	0.04	2.9	0.0		0.0		80.0	0.111	3−6	27 468
V	1.2	8.3	1.2	17.2	1.2	76.5	6.4	7.9	0.02	3.5	0.0		0.0		90.0	0.100	3−6	25 396
W	0.0		6.0	15.8	12.0	76.7	32.0	7.4	0.10	3.2	49.9	0.096	0.0		0.0			25 906
X	0.0		12.0	16.5	6.0	76.7	31.9	7.9	0.10	3.1	0.0		0.0		50.0	0.089	5−7	40 132
Y	0.0		6.0	16.6	12.0	76.6	31.9	7.9	0.10	3.3	0.0		0.0		50.0	0.098	5−7	45 094
Z	0.0		12.0	16.3	6.0	76.7	0.0		0.10	2.9	0.0		31.9	6.7	50.0	0.082	5−7	48 567

[a] The columns for each type of move (reptation, end rotation, flip, concerted rotation, volume fluctuation, end bridging, directed internal bridging, and directed end bridging) give the percentage contribution of moves to the MC mix and the acceptance ratio for that move, respectively. Run B used no directing potential, and run D used directing potential II, while all other DEB runs used directing potential I, as shown in Figure 2.

To circumvent this difficulty, and provide a stringent measure of the local relaxation rate, we use the second neighbor vector autocorrelation function (N2V−ACF) defined by the C−C−C chord,[39]

$$f_2(t) = \frac{3}{2}\langle(\mathbf{b}_i(t+t_0)\cdot\mathbf{b}_i(t_0))^2\rangle - \frac{1}{2} \qquad (26)$$

where $\mathbf{b}_i$ denotes the unit vector from atom $i-1$ to its second neighbor atom $i+1$, and both atoms are in turn nearest neighbors of atom i. Note that a connectivity altering move which reverses the sequence numbers of atoms $i-1$, i, and $i+1$, will cause the deduced identities of atoms $i-1$ and $i+1$ to be exchanged. This causes the direction of the vector $\mathbf{b}_i$ to be reversed, which has zero effect on the above autocorrelation function.

To characterize the relaxation of the large scale degrees of freedom associated with the global chain configurations, two further measures can also be used. The mean squared displacement function of the chain center of mass $\mathbf{x}_{COM}$ (COM−MSD) is evaluated by ensemble averaging over all n chains, using the expression

$$f_c(t) = \langle(\mathbf{x}_{COM}(t+t_0) - \mathbf{x}_{COM}(t_0))^2\rangle \qquad (27)$$

The autocorrelation function of the chain end-to-end vector (EEV−ACF) is given by

$$f_e(t) = \langle\mathbf{e}(t+t_0)\cdot\mathbf{e}(t_0)\rangle \qquad (28)$$

where $\mathbf{e}$ denotes the vector from the first to the last atom in the specified chain, normalized as a unit vector. The COM−MSD reflects the rate of generation of new chain configurations in terms of an *effective* chain motion. The EEV−ACF is a less quantitative, but more physically intuitive measure of the rate at which the memory of existing chain configurations is erased.

The simulations reported here have many different "mixes" of MC move algorithms, in which some moves are more computationally expensive than others. Hence the time correlation functions are scaled so that the time axis corresponds to the CPU time taken for each run. Since each data set corresponds to a total of 10^7 steps, the relaxation rate per MC step can also be inferred by inspection of these time correlation functions. The exception is the run (F) with 61.8% DIB moves, which required nearly 70 000 s.

All of the time correlation functions are evaluated over 100 saved configurations by averaging over multiple time origins, with no additional smoothing. Hence the EEV−ACF's in particular become increasingly noisy at long times, due to the reduced number of time origins for each ensemble average. Nevertheless, they are displayed here over their maximum time range, to aid in identifying the different curves and their associated total CPU times. It should also be emphasized that the time correlation functions are used here purely to assess the performance of the MC sampling procedures, with no attempt to quantitatively interpret the artificial dynamics of the atoms.

Validation

To verify that eqs 12 and 14 and all associated expressions are correctly derived and implemented, the same code was used to perform a series of test simulations on "phantom" chain systems. Such chains are defined using the polyethylene bond geometry, but without the nonbond interactions, and with or without the torsion potential terms. Suitable statistics for stringent ratification of the algorithms can be obtained efficiently by using a fixed volume system of 10 chains

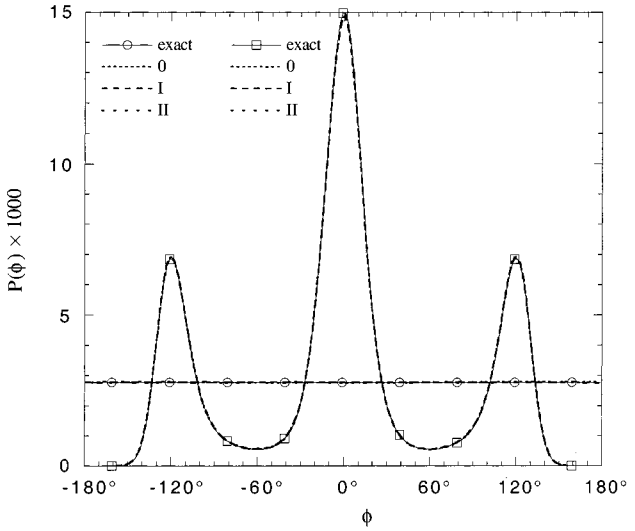

Figure 3. Distribution of torsion angles for MC simulations of noninteracting "phantom" chains. The solid lines represent the exact analytical distributions, with and without the torsional potential (squares and circles respectively). The dashed lines represent simulation results using the directing potential variants I and II depicted in Figure 2 and with no directing potential (0).

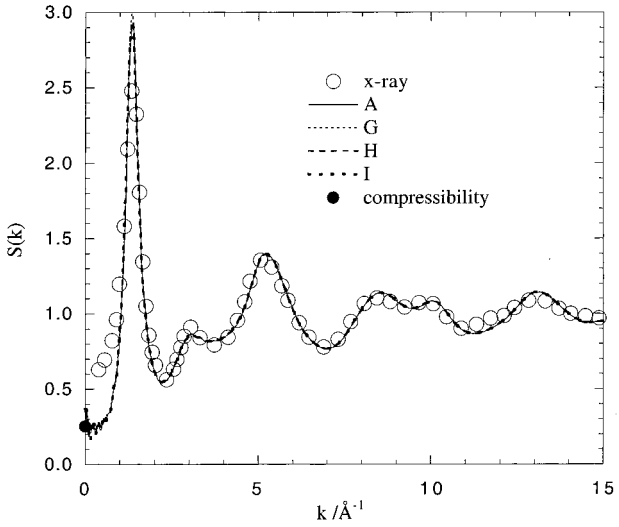

Figure 4. Calculated total static structure factor $S(k)$ for C_{1000} polyethylene melts at 450 K, simulated by Monte Carlo including DIB moves (run G), DEB moves (H), both (I), and neither (A). The open circles represent X-ray diffraction data[41] for C_{6400} polyethylene at 430 K. The closed circles at $k = 0$ correspond to the value derived from the simulated or experimental[43] isothermal compressibility.

containing a total of 200 united atoms. The MC mix consists of 1.2% reptation moves, 1.2% end rotations, 7.6% DIB moves ($l = 3-8$) and 90% DEB moves ($l = 4-7$). Each run is of ~20 CPU hours duration, corresponding to 120−160 million MC steps.

Torsion angle distributions for the phantom chain simulations are given in Figure 3, using the described variants of the fictitious directing potential, which is specified in eq 16. The first series corresponds to chains with nonbond and torsion terms switched off. For these chains, an exactly uniform distribution of torsion angles is expected. The second series corresponds to chains with the Ryckaert−Bellemans torsion function, but without the nonbond interactions. For such chains, the expected torsion distribution can be derived analytically from the torsion potential. The figure depicts the torsion distributions obtained by simulations with a mixture of DIB and DEB moves of varying lengths, using both variants of the fictitious directing potential shown in Figure 2, or no directing potential. It can be seen that, in every case, the distribution obtained from the simulation is statistically indistinguishable from the correct analytical distribution. These results thus confirm the numerical rigor of our simulation algorithms and code. This validation is a particularly important step for algorithms which combine the elements of configuration bias, real and fictitious potential energy terms and geometrical bridging via explicit solution search.

The simple united atom model for linear polyethylene used in these simulations has previously been shown to give good agreement with a range of experimentally determined properties, including density, isothermal compressibility, structure factor, diffusivity and stress−optical coefficient.[15,26,40] For the present work we simply wish to establish that the new algorithms give the same system characteristics as the existing ones. The static structure factor $S(k)$ is a convenient and stringent test for this requirement. Figure 4 compares the static structure factor obtained with and without the directed bridging algorithms. Again it can be seen that the different curves are essentially indistinguishable.

The simulated structure factor also agrees well with the X-ray diffraction data of Honnell et al.[41] As the wavevector k approaches zero, the simulation $S(k)$ becomes somewhat noisy due to the finite system size. The intercept $S(0)$ can be defined more precisely via calculation of the isothermal compressibility.[1] The calculated compressibility of 1.2×10^{-9} Pa^{-1} matches experimental values of $(1.1-1.2) \times 10^{-9}$ Pa^{-1} at 450 K for various comparable PE grades.[42,43] The shape of the low-k region of our $S(k)$ also agrees with PRISM integral equation theory.[41] Hence the slight discrepancy with the measured X-ray $S(k)$ in this region could be due to the sensitivity of the low-k X-ray data to irregularities in the melt surface.[41]

Results

Figure 5 shows the acceptance ratio for DIB and DEB moves as a function of the number of displaced atoms. It can be seen that the acceptance ratio for DIB moves drops almost exponentially with increasing bridge length. For the DEB algorithm, moves with 5 bridging atoms have the highest acceptance. These acceptance ratios are somewhat higher than for conventional EB, implying that when new bridges are formed from a chain end into another chain, longer bridges can indeed be grown with less torsional strain. Also shown in the plot is the effective acceptance ratio for DEB, discounting trial moves that can be rejected instantly. These include attempted moves where the selected end has no target sites to attack, where the target site is too close to the end of its own chain or where the new chain lengths fall outside the bounds of the prescribed molecular weight distribution. It can be seen that roughly half of all DEB moves are rejected instantly in this way, requiring negligible CPU time. Hence the effective acceptance ratio for DEB is approximately double the measured value, and reaches a maximum of around 0.3% for five-atom bridges. Note that this is still very low when compared with most MC moves commonly used in condensed matter simulations. The proportion of EB moves which can be rejected instantly (not shown) is also about 50%.

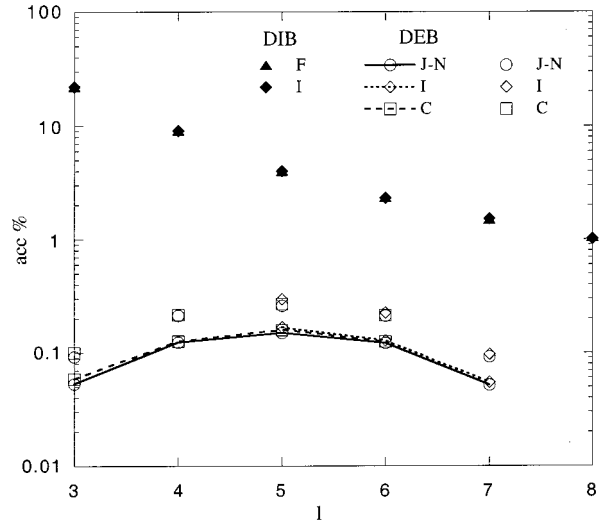

Figure 5. Acceptance ratio vs bridge length l for DIB and DEB polyethylene simulations. Closed symbols denote DIB acceptance ratios, while open symbols with and without connecting lines represent DEB acceptance ratios with and without instantly discarded moves, respectively. Points are for runs J, K, L, M, N (denoted J−N), F, I, and C, as specified in Table 1.

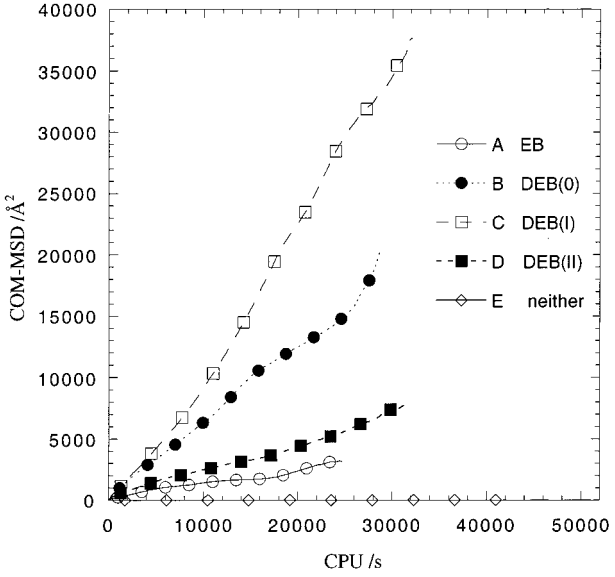

Figure 6. Mean squared displacement of the chain centers of mass during MC simulations of polyethylene, using EB moves (run A), DEB moves (l = 3−6) with no directing potential (B), DEB moves (l = 3−6) with directing potentials I (C) and II (D), and no variable connectivity moves (E). Symbols used to distinguish curves are drawn at intervals of 10 data points.

In Figure 6, we show the center of mass mean squared displacement functions for a number of different variable-connectivity run protocols and compare them with a fixed-connectivity run with predominantly ConRot moves. A dramatic difference is observed between the fixed-connectivity run, and the run where EB moves are added to the same mix of MC moves. In the same figure we also show the equivalent data for three different DEB simulations, utilizing the different variants of the fictitious biasing potential. It can be seen that the DEB method is clearly superior to the EB method in each case. The optimum potential, variant I, yields a COM−MSD rate which is approximately 10 times more efficient than EB, and some 5−6 orders of magnitude

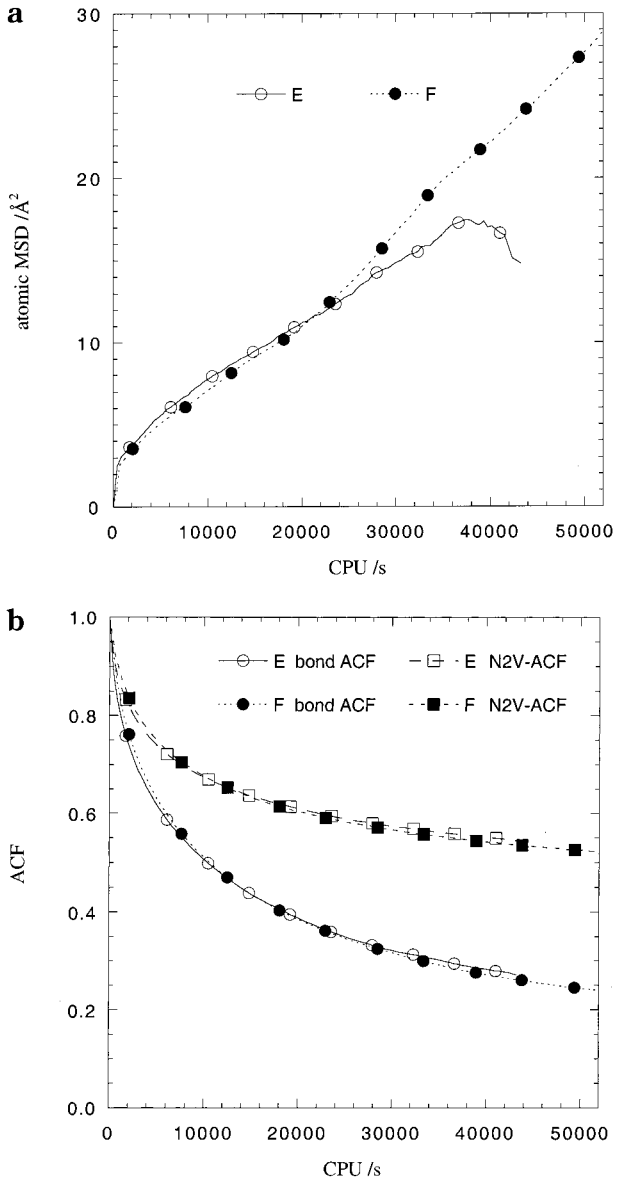

Figure 7. Local equilibration measures for MC simulations of polyethylene, using ConRot (run E) or DIB (run F), with no variable connectivity moves: (a) atomic mean squared displacement functions; (b) first neighbor (bond) and second neighbor vector autocorrelation functions.

faster than the fixed-connectivity simulation. The "undirected" DEB simulation, with no FENE directing potential, is only moderately less efficient. The implication here is that the choice of an optimum bias potential is beneficial but not crucial to the success of this algorithm. Given that the purpose of the fictitious potential is to direct the regrowth of the new chain section, it appears that for a dense melt environment, this regrowth is already governed by the favorable shape of the free volume "tube" formed when the original section is removed. Interestingly, variant II of the directing potential is seen to be less efficient than no directing potential at all, at least when the present fictitious potential parameter values are used.

To assess the value of the DIB algorithm, we need to compare its performance to the ConRot algorithm in a conventional, fixed-connectivity NpT simulation. Figure 7a compares the calculated atomic mean squared displacements for two such runs, where the DIB run involves displacements of 3−8 atoms. Figure 7b depicts

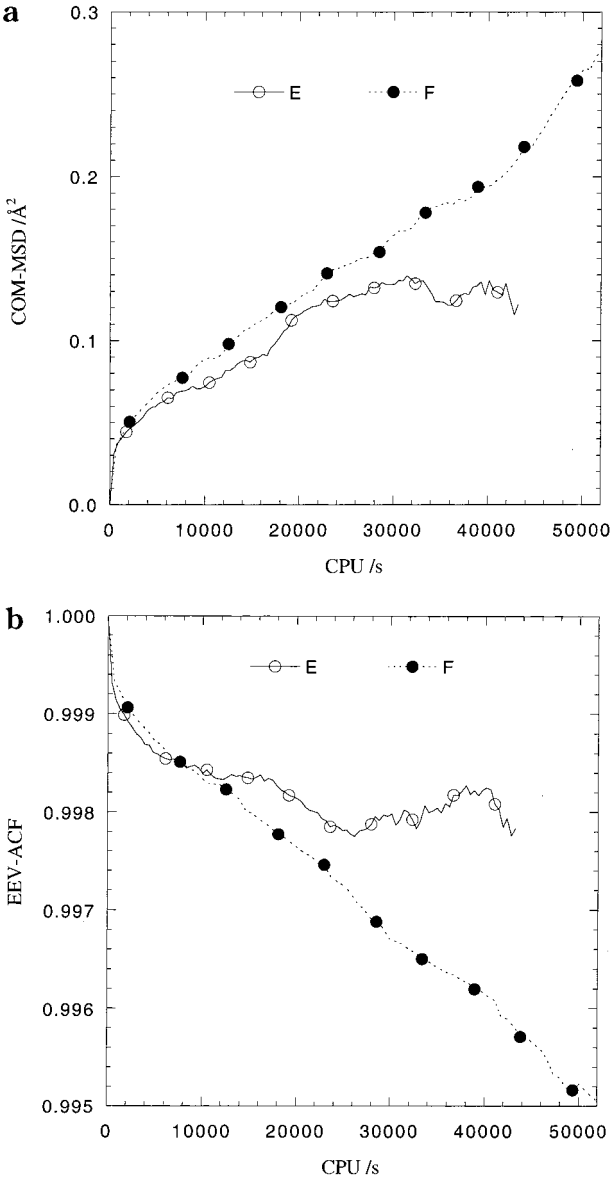

Figure 8. Global equilibration measures for MC simulations of polyethylene, using ConRot (run E) or DIB (run F), with no variable connectivity moves: (a) mean squared displacement functions for the chain centers of mass; (b) autocorrelation functions for the chain end-to-end vectors.

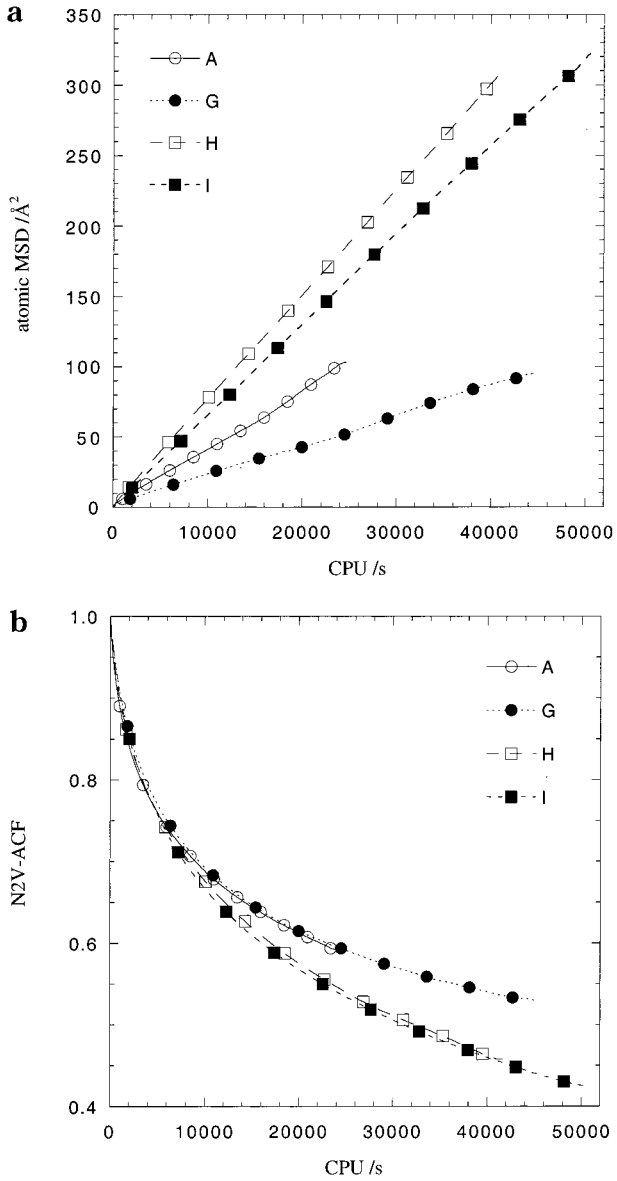

Figure 9. (a) Atomic mean squared displacement and (b) second neighbor vector autocorrelation functions for variable connectivity MC simulations of polyethylene, using move mixes with ConRot/EB moves (run A), DIB/EB (G), ConRot/DEB (H), and DIB/DEB(I).

the second neighbor vector autocorrelation functions for the same runs. Also shown are the corresponding autocorrelation functions for nearest neighbor vectors, i.e., bond vectors. The former decay more slowly than the latter, reflecting the tetrahedral geometry and the nature of the gauche−trans conformational transitions that occur in polyethylene.

From Figure 7, we see that the relaxation rates in the two different runs are virtually identical, according to all three measures used. The DIB algorithm provides more vigorous sampling per MC step, by displacing more atoms. However DIB also has a higher computational cost per step. These two factors cancel each other almost exactly in the present case.

Figure 8 shows the COM−MSD's and chain end-to-end vector autocorrelation functions for the ConRot and DIB runs. The two algorithms again exhibit very similar performances. Note that the observed rate of displacement of entire chains is considerably slower than that of individual atoms. An effective chain diffusion coefficient could perhaps be inferred from the vaguely linear region of Figure 8a, but the average displacement of each chain over an entire run is only a fraction of an atomic diameter. The observed decay in the EEV−ACF's is negligible, implying that the chain end-to-end vectors at the end of each run are virtually identical to what they were at the beginning of the run. Thus, no significant relaxation of the global chain conformations has occurred.

We should now consider the relative performance of DIB and ConRot in the presence of connectivity-altering MC moves. Figure 9a displays the atomic MSD plots for the four different combinations of ConRot/DIB plus EB/DEB simulations. By comparing it with Figure 7a, it is apparent that variable connectivity moves enhance the diffusion rate of individual atoms by up to an order of magnitude, an effect that is explored more fully later in this section. The diffusion rate is also noticeably higher for the DEB runs than for the EB runs.

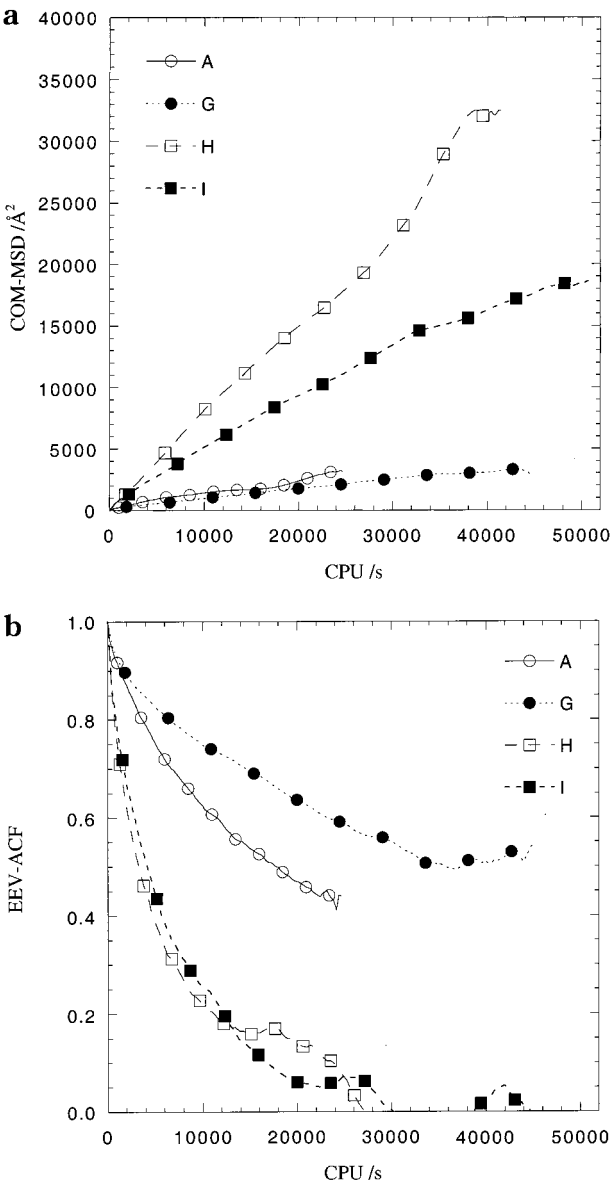

Figure 10. (a) Chain center of mass mean squared displacement and (b) chain end-to-end vector autocorrelation functions for variable connectivity MC simulations of polyethylene, using move mixes with ConRot/EB moves (run A), DIB/EB (G), ConRot/DEB (H), and DIB/DEB(I).

Figure 9b shows the N2V−ACF plots for the same four runs. Here the observed relaxation rates are more comparable to those depicted in Figure 7b for the fixed connectivity simulations. Again the performance of the DEB runs is somewhat superior to the EB runs, notably at longer times. Figure 10 displays the COM−MSD and EEV−ACF plots for the four ConRot/DIB plus EB/DEB combination runs. In each case, DEB proves to be markedly superior to EB, as seen previously in Figure 6.

Comparing DIB with ConRot in Figures 9 and 10, it can be seen that DIB leads to faster decorrelation of second neighbor vectors per MC step than ConRot, but that this enhancement is canceled by the increased CPU time per MC step, much as is seen for fixed connectivity simulations. However, the other equilibration measures do not reveal any noticeable improvement in the relaxation rate per MC step when using DIB instead of ConRot. Since the DIB algorithm still requires greater CPU time per step, it is clearly somewhat inferior to ConRot when used in variable connectivity simulations. This conclusion reflects the diminished importance of both moves, when they are used in combination with variable connectivity moves.

Figures 9 and 10 can also be used to assess the role of the connectivity-altering moves in sampling local and global configurations. We see that the chain centers of mass are displaced much faster than the individual atoms. The average effective displacement for each chain during a run is 50−180 Å. For comparison, the observed average chain end-to-end distance and radius of gyration are on the order of 140 and 55 Å, respectively (for C_{1000} chains). Figure 10 shows that 10 million iterations of the DEB MC mix are sufficient for full decorrelation of the global chain configurations.

So far we have established that the combination of ConRot and DEB provides the most efficient means of relaxing this model polymer melt. Next, we need to identify the optimal form of the DEB moves. It is already apparent that MC acceptance ratio is a poor indicator of simulation efficiency for these elaborate mixed MC protocols. While Figure 3 suggests that five-atom DEB moves are optimal, the best test is to perform full comparative simulations.

Figures 11 and 12 show the atomic MSD, N2V−ACF, COM−MSD, and EEV−ACF results obtained for DEB simulations with various DEB bridge lengths l. Note that the $l = 3$ DEB move is essentially equivalent to conventional EB, the main difference being that the list of candidate moves is defined using a different target atom. Simulations with bridge lengths of four, five, and six atoms display similar efficiency. Three is the minimum number of atoms that can be used for bridging moves with predefined bond lengths and angles. $l = 7$ appears to be the upper limit for efficient sampling using this formalism and polymer model. Further increases in bridge length not only cost more CPU time per MC step but also suffer from a reduced acceptance rate. It is interesting that a range of bridge lengths (e.g., $l = 3-6$) appears to be slightly more efficient than a single length. One may surmise that a larger range of segment lengths reduces the likelihood of direct reversal or "shuttling" of DEB moves. It is apparent from the N2V−ACF results that no significant change in the rate of local torsional relaxation is observed on varying the DEB segment length.

The variable connectivity simulations discussed to date have all contained 50% connectivity-altering moves. This ratio has stemmed from earlier work with the EB method.[12,15,24] For EB simulations, it is still the long-range configurational characteristics which exhibit the slowest relaxation,[15] thus governing the equilibration over all length scales. The DEB results presented here indicate that the chain end-to-end vector orientations can now be made to equilibrate faster than the individual bond orientations. Hence we should readdress the question of the optimum ratio of DEB moves to other MC moves.

Figures 13 and 14 show the atomic MSD, N2V−ACF, COM−MSD, and EEV−ACF for a series of runs with varying DEB move fractions. From Figure 14, we see that the global chain relaxation rate reaches its optimal value with about 50% DEB moves; increasing this fraction further does not lead to any significant improvement. Indeed, full regeneration of the chain end-to-end vectors can be achieved within $\sim 10^7$ MC steps with only 20% DEB moves. Conversely, the second

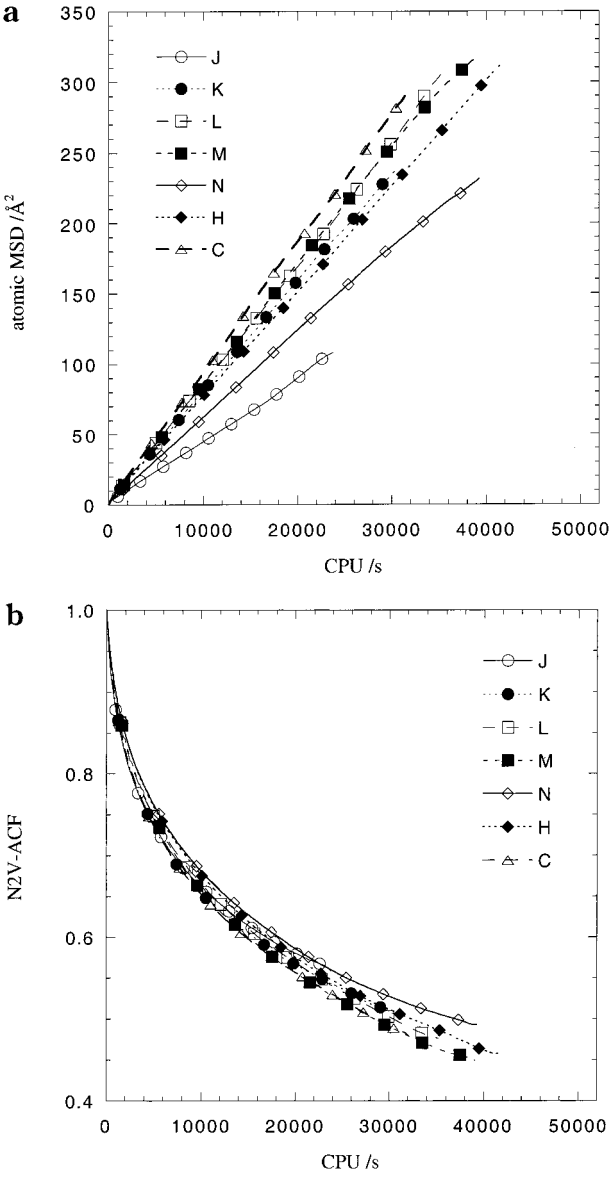

Figure 11. (a) Atomic mean squared displacement and (b) second neighbor vector autocorrelation functions for variable connectivity MC simulations of polyethylene, using DEB moves with bridge lengths l = 3 (run J), 4 (K), 5 (L), 6 (M), 7 (N), 5−7 (H), and 3−6 (C).

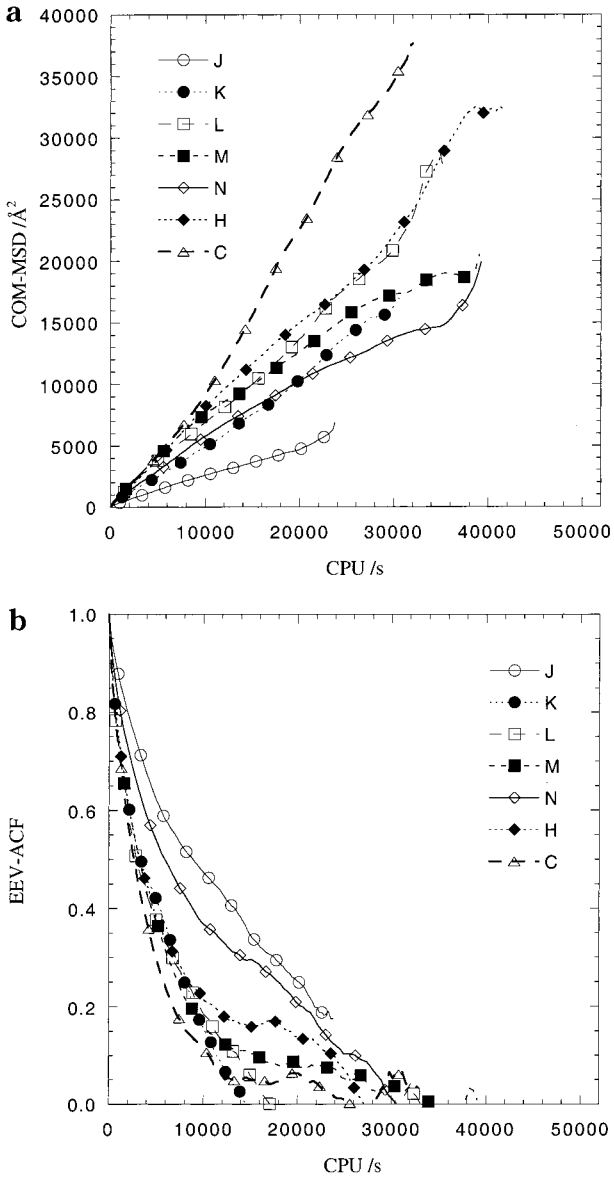

Figure 12. (a) Chain center of mass mean squared displacement and (b) chain end-to-end vector autocorrelation functions for variable connectivity MC simulations of polyethylene, using DEB moves with bridge lengths l = 3 (run J), 4 (K), 5 (L), 6 (M), 7 (N), 5−7 (H), and 3−6 (C).

neighbor vectors are not fully decorrelated after 10^7 steps, but the decay rate is very similar for all runs where the DEB fraction is between 30% and 70%. Thus, the simulation efficiency is rather insensitive to the fraction of DEB moves used, with 50−70% appearing to be the optimal range overall.

The final series of comparisons considered in this work is the effect of including or excluding reptation moves from variable connectivity simulations. Four runs are described, each with a typical MC move protocol, except for the replacement of reptations by other MC moves. In two of the runs, the replacement moves are flip moves. In the remaining two runs, the reptations are replaced by end rotation moves, in an attempt to increase the range of target atoms for end-bridging moves. The other variables are a choice between ConRot and DIB and a choice between EB and DEB.

Figure 15 shows the atomic MSD and N2V−ACF curves for the four reptation-free runs. The atom displacement plots are profoundly different to those previously reported. First, the curves are not linear, so the motion of individual atoms cannot be described by a diffusive analogue. Second, the actual displacements are greatly reduced. Clearly the reptation algorithm is by far the most efficient mechanism for transfer of mass in these simulations. Conversely, the N2V−ACF curves differ only marginally from those obtained with reptation moves, as seen for example in Figure 9b. Somewhat slower relaxation is observed for EB than for DEB, notably for the MSD, while the other variations (end rotation/flip, ConRot/DIB) have little effect.

These observations are further reinforced by the COM−MSD's and EEV−ACF's of the reptation-free runs, which are shown in Figure 16. Relaxation of the global chain configurations is still very efficient, but less efficient than when reptation is included. Again the reduction in efficiency is rather more pronounced for the EB run than for the DEB runs.

Several conclusions may be drawn from the reptation-free results. The obvious one is that reptation is the

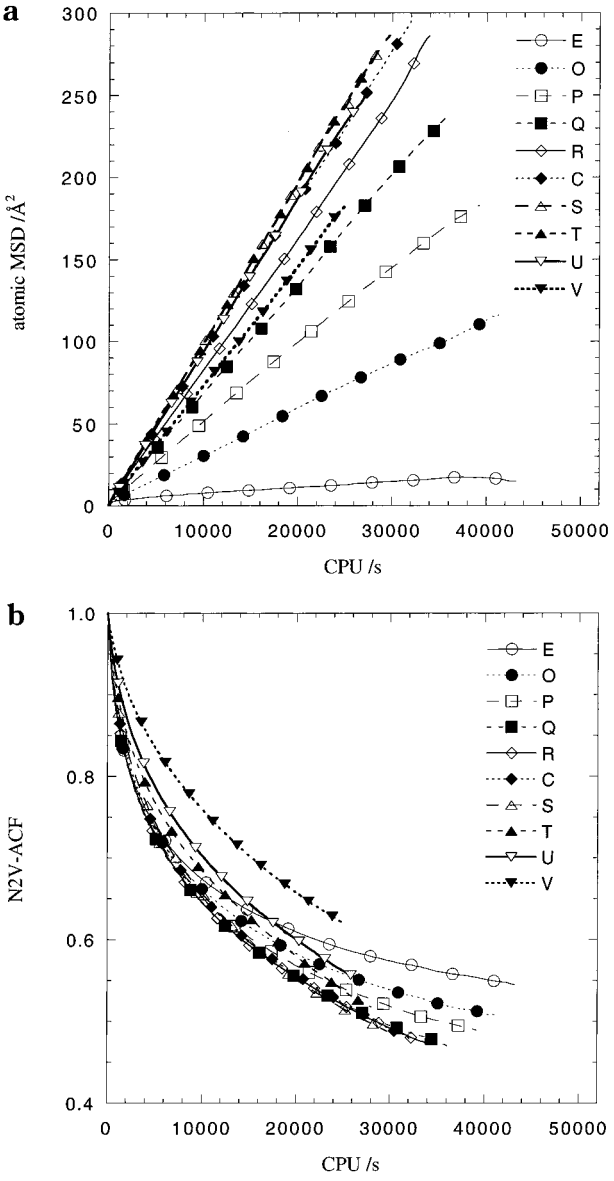

Figure 13. (a) Atomic mean squared displacement and (b) second neighbor vector autocorrelation functions for MC simulations of polyethylene. E, O, P, Q, R, C, S, T, U, and V represent runs containing 0, 10, 20, 30, 40, 50, 60, 70, 80, and 90% DEB moves.

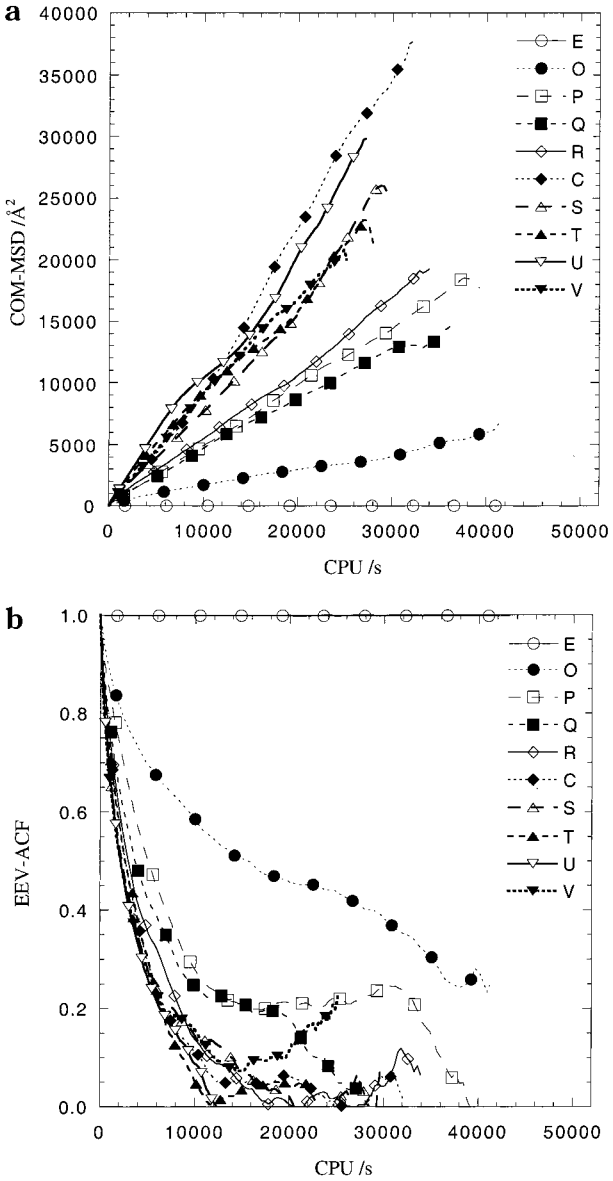

Figure 14. (a) Chain center of mass mean squared displacement and (b) chain end-to-end vector autocorrelation functions for MC simulations of polyethylene. E, O, P, Q, R, C, S, T, U, and V represent runs containing 0, 10, 20, 30, 40, 50, 60, 70, 80, and 90% DEB moves.

fastest mechanism for actually displacing atoms. Hence the reported atomic MSD curves for each run reflect the efficiency of reptation moves in that run. Conversely the COM−MSD (and EEV−ACF) curves are dominated by the connectivity-altering moves, and reflect the efficiency of these moves. The N2V−ACF curves reflect the efficiency of torsional sampling, which is governed largely by ConRot or DIB moves.

From Figures 7a, 9a, and 13a, we may then further deduce that connectivity-altering moves dramatically increase the efficiency of reptation moves. Figures 10a and 16a demonstrate that reptation moves significantly enhance the efficiency of the end-bridging moves (EB more so than DEB). Thus, reptation and end-bridging moves complement each other synergistically. Note that the actual move acceptance ratios are virtually unaffected by this synergy.

In a polymer melt simulation consisting entirely of reptation moves, the equilibration rate is strongly dependent on the chain length (the scaling exponent of the longest relaxation time is approximately 3.25).[44] This is due to the high probability of move reversals or shuttling, caused by the shortage of free volume available for successive atom addition in one direction. Thus, a large proportion of the accepted reptation moves simply cancel each other out. In an EB simulation, the finite number of chain ends present means that only a small set of candidate EB moves are energetically feasible at any time. This, too, leads to a pronounced shuttling effect. Clearly the combination of reptation and EB moves reduces the incidence of shuttling in both cases.

The reptation results also help clarify the differences between EB and DEB results. Relative to EB, each DEB move displaces a larger number of atoms, and has a higher acceptance ratio, but costs more CPU time. Solely on the basis of these factors, one might expect the COM−MSD rates depicted in Figures 10 and 16 to be approximately 2 times larger for DEB than for EB. The observed difference is approximately an order of mag-

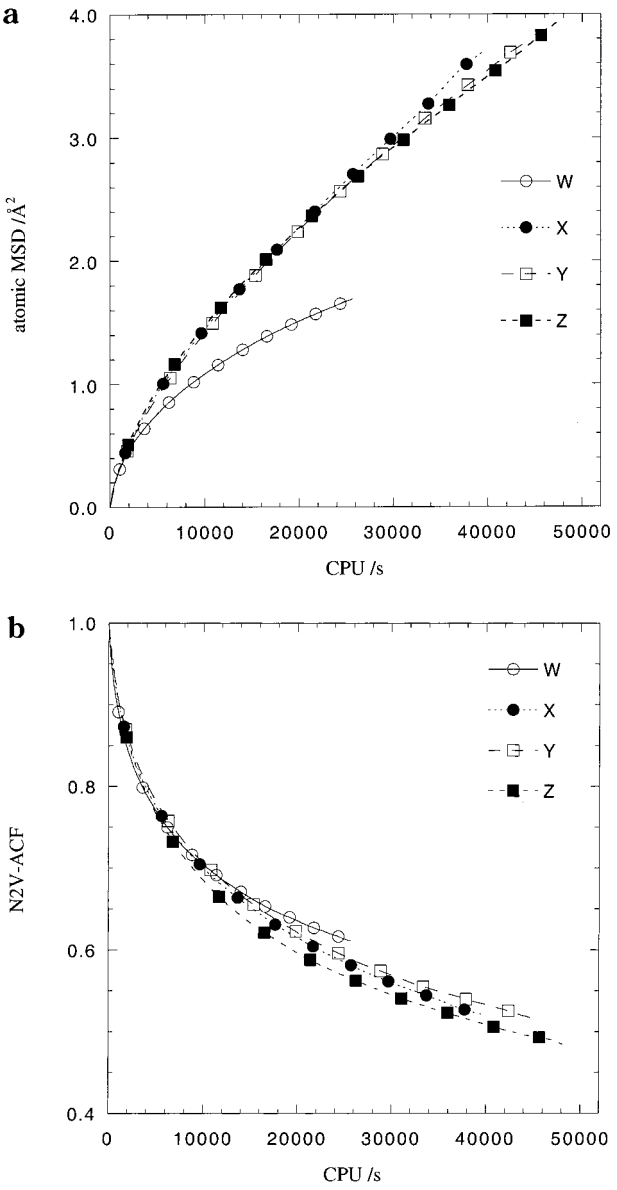

Figure 15. (a) Atomic mean squared displacement and (b) second neighbor vector autocorrelation functions for reptation-free variable connectivity MC simulations of polyethylene, with reptation moves replaced by extra flip moves (runs W, Y) or end rotation moves (X, Z). The MC mixes include ConRot/EB (run W), ConRot/DEB (X, Y), and DIB/DEB moves (Z).

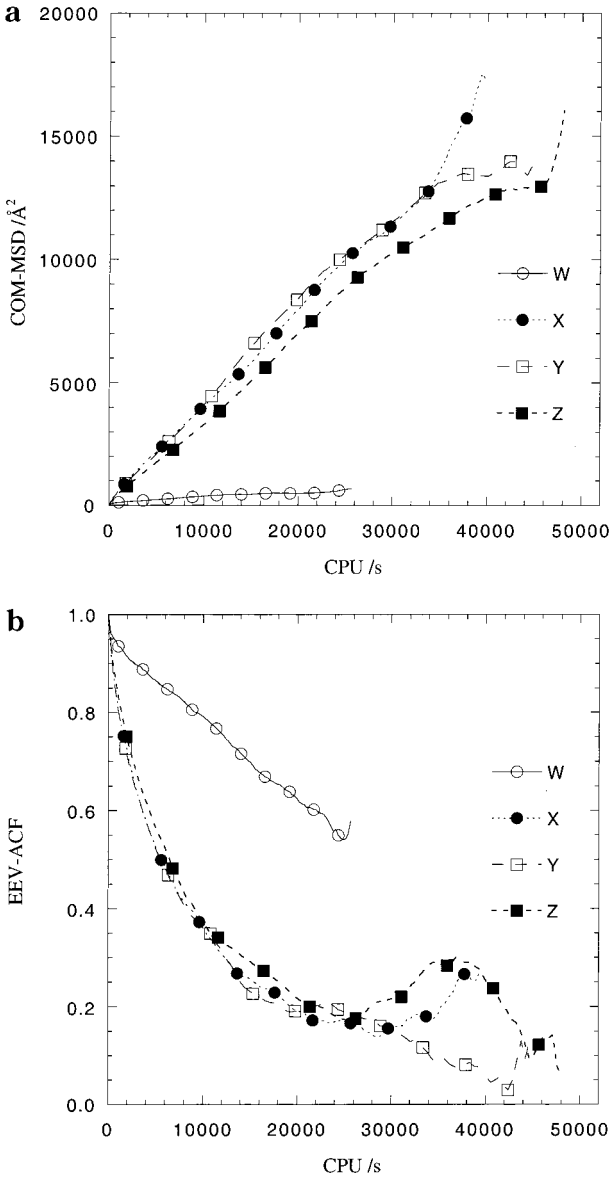

Figure 16. (a) Chain center of mass mean squared displacement and (b) chain end-to-end vector autocorrelation functions for reptation-free variable connectivity MC simulations of polyethylene, with reptation moves replaced by extra flip moves (runs W, Y) or end rotation moves (X, Z). The MC mixes include ConRot/EB (run W), ConRot/DEB (X, Y), and DIB/DEB moves (Z).

nitude, and is larger for simulations without reptations. This implies that the *main* advantage of DEB over EB is the reduced move shuttling, rather than the larger number of displaced atoms or the higher acceptance ratio.

This shuttling hypothesis can be tested by explicitly recording the identities of each atom displaced by reptation, EB, and DEB moves. For convenience each EB and DEB move is identified by a single atom, namely the target atom for the trimer bridge, while reptations are treated as single atom displacements without any chain renumbering. Then we simply count (i) the total number of atoms so identified over the course of the run and (ii) the maximum number of times any one atom is identified and express each quantity in terms of a ratio over the total number of moves of that type.

Results for selected simulation runs are given in Table 2. Shuttling can be detected by the restriction of successful moves to a small fraction of atoms, or conversely by a high frequency of repeated displacements of the same atom. In the absence of EB or DEB moves, the ratio of reptated atoms to reptation moves of 0.003 (248 out of 24 000 atoms in 77 879 accepted moves) is clearly very small. This ratio is greatly enhanced by incorporating EB or DEB moves. It can also be confirmed that, when compared to DEB, successful EB moves are restricted to a smaller proportion of

Table 2. Selection of Individual Atoms for Reptation, End Bridging and Directed End Bridging Moves

		atoms per move			maximum repeats per move		
run	*l*	reptation	EB	DEB	reptation	EB	DEB
E		0.003			0.0232		
W	3		0.102			0.0178	
Y	5−7			0.447			0.0047
A	3	0.053	0.188		0.0050	0.0061	
H	5−7	0.061		0.504	0.0036		0.0032
L	5	0.061		0.381	0.0048		0.0033

atoms, and that this proportion is enhanced more significantly by incorporating reptation moves. The comparison of runs L and H is not conclusive, but it does suggest that increasing the range of bridge lengths l from 5 to 5−7 also reduces shuttling slightly in DEB and reptation moves.

The ability to perform polymer MC simulations with reduced or no reliance on reptation moves is important if these techniques are to be applied to more complex polymer systems. The ability to add and delete individual backbone atoms is essentially unique to linear polyethylene. Even simple vinyl polymers require the insertion of significantly larger sections of backbone into a dense melt environment. Work currently in progress[25] indicates that this leads to dramatically reduced reptation efficiency. More complex systems such as branched polymers, block copolymers and functionalized polymers cannot undergo reptations at all, unless the addition or removal of end atoms is accompanied by a change in the chain composition and/or architecture.

The results given in Figures 15 and 16 show that entangled linear PE melts can still be equilibrated by DEB (or less effectively by EB), without recourse to reptation moves. The low atomic MSD in Figure 15 appears to show that the individual atoms have not moved far enough to fully sample the configuration space. However, in this molecular system, the presence of connectivity-altering moves means that all atoms are in fact equivalent. For such systems, the required condition for equilibration is a mean displacement on the order of an atomic radius or greater.[1] This is in stark contrast to a conventional fixed connectivity polymer simulation, where atoms with different sequence numbers are nonequivalent, and must move much greater distances to ensure full sampling of the configuration space.

Conclusions and Future Prospects

We have introduced new directed bridging algorithms for quantitative atomistic Monte Carlo simulations of high polymer melts, using reasonably realistic, fully entangled melts of linear polyethylene as a test case. The effectiveness of the DIB algorithm is comparable with, but not superior to, the previously developed ConRot method. However, the DEB algorithm is clearly superior to the earlier end-bridging algorithm, with performance enhancements of around an order of magnitude. DEB can thus be identified as the current method of choice for equilibration of such high polymer systems on all length scales.

The effectiveness of the DEB algorithm is relatively insensitive to the specific details of the algorithm implementation, such as the ratio of DEB to other MC moves, the number of atoms displaced in each move, or the choice of the directing potential. It is also much less reliant on the presence of reptation moves than EB, implying that it will be more suitable for application to more chemically complex polymer systems.

In previous polymer simulations, the total time required for full equilibration has been governed by the time required to relax the global chain conformational characteristics. Significantly, DEB simulations allow these characteristics to equilibrate at a faster rate than the local or short range conformational characteristics. Hence the advantage of DEB simulations over conventional fixed connectivity techniques increases dramatically with increasing chain length.

We are currently combining these advanced simulation techniques with new parallelisation methods to enable the efficient characterization of much larger polyethylene systems, involving some 200 000 atoms and molecular weights which match commercial grade HDPE materials.[45] Thus, the long-standing goal of achieving definitive atomic-level characterization of genuine, technologically relevant high polymers is now within reach.

Acknowledgment. The authors wish to thank Graeme Moad (CSIRO) and Per Nyberg (NEC) for their help in initiating this work, and Stephen Leak (NEC) for assistance with code optimization. Computational resources provided by the High Performance Computing and Communications Centre (HPCCC) and the Cooperative Research Centre for Polymers (CRC-P) are gratefully acknowledged.

References and Notes

(1) Allen, M. P.; Tildesley, D. J. *Computer Simulation of Liquids*; Clarendon Press: Oxford, England, 1987.
(2) Frenkel, D.; Smit, B. *Understanding Molecular Simulation*; Academic Press: San Diego, CA, 1996.
(3) Leach, A. R. *Molecular Modelling: Principles and Applications*; Addison-Wesley Longman: Harlow, England, 1996.
(4) Sadus, R. J. *Molecular Simulation of Fluids*; Elsevier: Amsterdam, 1999.
(5) Gubbins, K. E., Quirke, N., Eds. *Molecular Simulation and Industrial Applications*; Gordon & Breach: Amsterdam, 1996.
(6) Deem, M. W. *AIChE J.* **1998**, *44*, 2569.
(7) Uhlherr, A.; Theodorou, D. N. *Curr. Opin. Solid State Mater. Sci.* **1998**, *3*, 544.
(8) Roe, R. J., Ed. *Computer Simulation of Polymers*; Prentice Hall: Englewood Cliffs, NJ, 1991.
(9) Binder, K., Ed. *Monte Carlo and Molecular Dynamics Simulations in Polymer Science*; Oxford University Press: New York, 1995.
(10) Gelin, B. R. *Molecular Modeling of Polymer Structures and Properties*; Hanser: Munich, Germany, 1994.
(11) Leontidis, E.; Forrest, B. M.; Widmann, A. H.; Suter, U. W. *J. Chem. Soc., Faraday Trans.* **1995**, *91*, 2355.
(12) Mavrantzas, V. G.; Theodorou, D. N. *Macromolecules* **1998**, *31*, 6310.
(13) Jin, Y.; Boyd, R. H. *J. Chem. Phys.* **1998**, *108*, 9912.
(14) Balijepalli, S.; Rutledge, G. C. *Macromol. Symp.* **1998**, *133*, 71.
(15) Mavrantzas, V. G.; Boone, T. D.; Zervopoulou, E.; Theodorou, D. N. *Macromolecules* **1999**, *32*, 5072.
(16) Dodd, L. R.; Boone, T. D.; Theodorou, D. N. *Mol. Phys.* **1993**, *78*, 961.
(17) Leontidis, E.; de Pablo, J. J.; Laso, M.; Suter, U. W. *Adv. Polym. Sci.* **1994**, *116*, 283.
(18) Deem, M. W.; Bader, J. S. *Mol. Phys.* **1996**, *87*, 1245.
(19) Baschnagel, J.; Binder, K.; Doruker, P.; Gusev, A. A.; Hahn, O.; Kremer, K.; Mattice, W. L.; Müller-Plathe, F.; Murat, M.; Paul, W.; Santos, S.; Suter, U. W.; Tries, V. *Adv. Polym. Sci.* **2000**, *152*, 41.
(20) Frenkel, D.; Mooij, G. C. A. M.; Smit, B. *J. Phys.: Condens. Matter* **1992**, *4*, 3053.
(21) de Pablo, J. J.; Laso, M.; Suter, U. W. *J. Chem. Phys.* **1992**, *96*, 2395.
(22) Uhlherr, A. *Macromolecules* **2000**, *33*, 1351.
(23) Wick, C. D.; Siepmann, J. I. *Macromolecules* **2000**, *33*, 7207.
(24) Pant, P. V. K.; Theodorou, D. N. *Macromolecules* **1995**, *28*, 7224.
(25) Doxastakis, M.; Mavrantzas, V. G.; Theodorou, D. N. Submitted to *J. Chem. Phys.*
(26) Harmandaris, V. A.; Mavrantzas, V. G.; Theodorou, D. N. *Macromolecules* **1998**, *31*, 7934.
(27) Mavrantzas, V. G.; Theodorou, D. N. *Macromol. Theory Simul.* **2000**, *9*, 500.
(28) Mavrantzas, V. G.; Öttinger, H. C. Submitted to *Phys. Rev. Lett.*
(29) Leontidis, E.; Suter, U. W. *Mol. Phys.* **1994**, *83*, 489.
(30) Uhlherr, A. *Comput. Theor. Polym. Sci.* **2000**, *10*, 29.
(31) Zervopoulou, E.; Schismenou, G.; Mavrantzas, V. G.; Theodorou, D. N. To be submitted to *Macromolecules*.

(32) Dijkstra, M.; Frenkel, D.; Hansen, J.-P. *J. Chem. Phys.* **1994**, *101*, 3179.
(33) Vendruscolo, M. *J. Chem. Phys.* **1997**, *106*, 2970.
(34) Uhlherr, A. To be published.
(35) Metropolis, N.; Rosenbluth, A. W.; Rosenbluth, M. N.; Teller, A. H.; Teller, E. *J. Chem. Phys.* **1953**, *21*, 1087.
(36) Rosenbluth, M. N.; Rosenbluth, A. W. *J. Chem. Phys.* **1955**, *23*, 356.
(37) Van der Ploeg, P.; Berendsen, H. J. C.; *J. Chem. Phys.* **1982**, *76*, 3271.
(38) Ryckaert, J.-P.; Bellemans, A. *Chem. Phys. Lett.* **1975**, *30*, 123.
(39) Smith, G. D.; Yoon, D. Y.; Jaffe, R. L. *Macromolecules* **1995**, *28*, 5897.
(40) Mavrantzas, V. G.; Theodorou, D. N. *Comput. Theor. Polym. Sci.* **2000**, *10*, 1.
(41) Honnell, K. G.; McCoy, J. D.; Curro, J. G.; Schweizer, K. S.; Narten, A. H.; Habenschuss, A. *J. Chem. Phys.* **1991**, *94*, 4659.
(42) Zoller, P. *J. Appl. Polym. Sci.* **1979**, *23*, 1051.
(43) Dee, G. T.; Ougizawa, T.; Walsh, D. J. *Polymer* **1992**, *33*, 3462.
(44) Deutsch, J. M. *Phys. Rev. Lett.* **1985**, *54*, 56.
(45) Uhlherr, A.; Leak, S. J.; Adam, N. E.; Nyberg, P. E.; Doxastakis, M.; Mavrantzas, V. G.; Theodorou, D. N. Submitted to *Comput. Phys. Comm.*.

MA0102060